β-decay properties of neutron-rich rare-earth isotopes

P. Sarriguren*
Instituto de Estructura de la Materia, IEM-CSIC, Serrano 123, E-28006 Madrid, Spain
(Received 21 July 2016; revised manuscript received 13 October 2016; published 4 January 2017)

In this paper, β-decay properties of even-even neutron-rich isotopes in the rare-earth mass region are studied within a microscopic theoretical approach based on a proton-neutron quasiparticle random-phase approximation. The underlying mean field is constructed self-consistently from a deformed Hartree-Fock calculation with Skyrme interactions and pairing correlations to which particle-hole and particle-particle residual interactions are added. Nuclei in this mass region participate in the astrophysical rapid neutron capture process and are directly involved in the generation of the rare-earth peak in the isotopic abundance pattern centered at $A \simeq 160$. The energy distributions of the Gamow-Teller strength as well as the β-decay half-lives and the β-delayed neutron-emission probabilities are discussed and compared with the available experimental information and with calculations based on different approaches.

DOI: 10.1103/PhysRevC.95.014304

I. INTRODUCTION

The astrophysical rapid neutron capture process (r process) is of fundamental importance to understand the nucleosynthesis of heavy neutron-rich nuclei and to account for their observed abundances [1–4]. It is believed that the process takes place in astrophysical explosive neutron-rich environments when the density of free neutrons is so high that the capture of neutrons by nuclei is the dominant mechanism and much faster than the competing β decay. However, the identification of the possible physical sites for the r process is still one major unsolved challenge. Neutron star mergers and neutrino-driven winds in core-collapse supernovae are two of the best suited scenarios (see [3,4] and references therein).

The path that the r process follows and the final pattern of isotopic abundances are the result of a complex network of reactions and decays competing with each other in changing conditions of densities and temperatures. Thus, to model the r process one needs reliable nuclear physics input for masses, neutron capture reaction rates, photodisintegration rates, β-decay half-lives ($T_{1/2}$), and β-delayed neutron-emission probabilities (P_n) for a large amount of nuclei ranging from the valley of stability to the neutron drip line.

The sensitivity of the final abundance pattern to the various nuclear properties and astrophysical conditions was largely studied (see, for example, Refs. [5,6] and references therein). The main conclusion is that given the astrophysical conditions, the final abundance pattern is basically determined by the nuclear properties of nuclei along the r-process path, as well as on the properties of nuclei involved in the freeze-out at the last stages of the process leading nuclei back to stability. In particular, the peaks found in the r-process abundance pattern at $A \simeq 80$, $A \simeq 130$, and $A \simeq 195$ are associated with the relatively large β-decay half-lives in the waiting point nuclei with closed neutron shells $N = 50$, $N = 82$, and $N = 126$, respectively. The matter accumulates at these points creating peaks in the observed abundances. At these points of extra stability the neutron capture becomes inhibited and the nucleosynthesis flow is highly influenced by the large β-decay half-lives that finally determine the time scale of the whole process.

Above $A \simeq 100$, in the region between the two main peaks at $A \simeq 130$ and $A \simeq 195$, there is also a smaller peak, which is away from closed neutron or proton shells. It appears at $A \simeq 160$ and is called the rare-earth peak. It was shown [7] that the rare-earth peak is generated during the last stages of the r process as nuclei decay to stability. The peak is mainly from the combined effects of nuclear deformation and β decay [7,8] and it is very sensitive to the nuclear properties of neutron-rich rare-earth isotopes of about 10–15 neutrons away from stability [5]. On the other hand, it was also argued that fission recycling with asymmetric fission fragment distributions may play a crucial role to understand the origin of the rare-earth peak [9]. This would emphasize the role of neutron star mergers as possible sites for the generation of the rare-earth peak. Thus, the characteristics of the rare-earth peak may offer unique insight into the late-time freeze-out behavior of the r process.

Unfortunately, it is difficult to measure the properties of nuclei far from the valley of stability involved in the r process because of the extremely low production yields in the laboratory. As a consequence, there is still little experimental information on the quantities needed for astrophysics. Although much progress is being made to measure masses and half-lives [10–14] and there are promising perspectives for the next future in the new facilities at FAIR [15], RIBF-RIKEN [16], and FRIB-MSU [17], the astrophysical simulations of the r process must still rely on extrapolations of the available data or on predictions from theoretical nuclear models. Obviously, these models must prove first their reliability by reproducing the available data, which in the case of decay properties means half-lives and Gamow-Teller strength distributions measured in the laboratory.

In medium and heavy mass nuclei, the shell model needs very large configuration spaces that exceed the present computation capabilities and the quasiparticle random-phase approximation (QRPA) was shown to be well suited to describe the properties of these nuclei and in particular, their

*p.sarriguren@csic.es

decay properties. QRPA calculations for neutron-rich nuclei have been performed in the past from spherical formalisms [18–20]. However, although the mass regions of interest mentioned above surrounding the magic neutron numbers $N = 50,82,126$ can be well described with such spherical formalisms, the r-process path crosses open-shell regions characterized by well-deformed shapes. Thus, deformed QRPA calculations, such as those in Refs. [21–32] have been developed. The sensitivity of the β-decay properties to nuclear deformation was proven in the above references, showing that these properties may differ substantially from the spherical assumption and that it is necessary to include the nuclear deformation for reliable estimates. The sensitivity to deformation of the GT strength distributions was exploited experimentally to be an additional source of information about the nuclear deformation, as it was shown in Ref. [33]. The effects of deformation on the decay properties of neutron-rich isotopes in medium-mass nuclei from Ge up to Pd have been studied in Refs. [29–31,34–36], demonstrating the need for theoretical formalisms accounting for nuclear deformation.

The rare-earth region, including nuclei in the range between $82 < N < 126$ and $50 < Z < 82$, is also well known to accommodate good rotors. However, very few studies of the decay properties of rare-earth nuclei are available yet. There are global calculations combining a microscopic QRPA approach for the GT response with the statistical gross theory for the first-forbidden (FF) decay [37]. There are also deformed QRPA calculations based on Woods-Saxon potentials and realistic CD-Bonn residual forces using the G matrix [38]. The finite-amplitude method was used in Ref. [39] to obtain a global description of the decay properties within a Skyrme QRPA with axial symmetry. Finally, a spherical relativistic formalism was used for a large-scale evaluation of the β-decay properties in r-process nuclei [40].

In this work I investigate the nuclear structure related to the decay properties in the region of neutron-rich rare-earth nuclei of interest for the r process [5] that includes Xe, Ba, Ce, Nd, Sm, Gd, and Dy isotopes with neutron numbers $86 < N < 126$. A theoretical formalism based on a deformed Skyrme HF+BCS+QRPA approach is used to calculate energy distributions of the Gamow-Teller strength for those isotopes and weighting properly the strength with phase-space factors, β-decay half-lives and β-delayed neutron-emission probabilities are calculated. The results are compared with the available experimental information on half-lives [41] and with other theoretical calculations [37–40]. Thus, after testing the capability of the method to reproduce the measured half-lives, predictions are made in more exotic nuclei including some of the isotopes that are planned to be measured in the future [15–17]. Also important for astrophysics are the GT strength distributions because they contain the underlying nuclear structure. Given that the phase factors in a stellar medium at high densities and temperatures may be quite different from the temperature in the laboratory, the stellar half-lives may also differ substantially from the laboratory half-lives because of the thermal population of the decaying nuclei and because the electron distribution in the stellar plasma might block the β-particle emission [42].

The article is arranged as follows: First, in Sec. II I review the theoretical formalism used in this work. Then, I show in Sec. III the results obtained for the self-consistent deformations in the neutron-rich isotopic chains of Xe, Ba, Ce, Nd, Sm, Gd, and Dy, together with the energy distributions of the Gamow-Teller (GT) strength at the corresponding equilibrium deformations. I also calculate β-decay half-lives and probabilities for β-delayed neutron emission, comparing the results with experimental data and with results from other calculations. Section IV summarizes the main conclusions.

II. THEORETICAL FORMALISM

The theoretical formalism used in this work to study the decay properties of neutron-rich isotopes was already introduced elsewhere [25–28] and I only sketch here the main points. The method starts from a self-consistent Hartree-Fock (HF) mean-field calculation with Skyrme interactions that includes pairing correlations and deformation. The calculations are performed with the force SLy4 [43], which is a suitable representative of the Skyrme forces. The fitting protocol of the parameters includes nuclear properties of unstable nuclei. The sensitivity of the decay properties to different choices of the underlying effective force is not critical and was studied elsewhere [25–28,44]. The single-particle wave functions are expanded in terms of the eigenstates of an axially symmetric harmonic oscillator in cylindrical coordinates, using 12 major shells. Pairing between like nucleons is considered in the BCS approximation by solving the BCS equations after each HF iteration, using fixed gap parameters which are determined from the experimental odd-even mass differences when this information is available [41]. When the masses are unknown the same pairing gaps as the closer isotopes measured are used. The method provides naturally the self-consistent equilibrium deformations that minimize the energy and there is no need to introduce any extra parameter.

In a next step, a spin-isospin residual interaction is added to the mean field and treated in a deformed proton-neutron QRPA [21–23,25,26,37]. The residual interaction contains two components acting in the particle-hole (ph) and in the particle-particle (pp) channels. The former can be derived consistently from the same Skyrme interaction used in the mean-field calculation in terms of the second derivatives of the energy density functional with respect to the one-body densities. To simplify the calculation, the ph residual force is expressed in a separable form [25,26]. This is a repulsive interaction that redistributes the GT strength by reducing and moving it to higher excitation energies and thus, shifting the GT resonance. The coupling strength is usually taken to reproduce the location of the GT resonance [22,25,26]. Based on previous work, the value $\chi_{\rm GT}^{ph} = 0.15$ MeV is taken here. The pp part is also introduced as a separable force [23]. It is attractive and moves the GT strength to lower excitation energies. Its coupling strength is usually fitted to reproduce the experimental half-lives [22]. Based on previous calculations (see Refs. [45,46] and references therein), the value $\kappa_{\rm GT}^{pp} = 0.03$ MeV is taken. One could fit these two coupling constants to reproduce the measured half-lives of particular nuclei, but because the aim here is to test the ability

of the method to account for the decay properties in a global way, I use the same coupling strengths for all the nuclei considered in this work.

The suitability of the separable forces was tested in Refs. [29,47,48] by comparing the results obtained from QRPA using deformed Woods-Saxon potentials and realistic CD-Bonn residual forces with similar calculations with separable forces. It was shown that separable forces still keep the main characteristic of realistic residual forces, concluding that both approaches, realistic and separable, lead to similar results.

Introducing the proton-neutron QRPA phonon operator that creates a GT excitation in an even-even nuclei as

$$\Gamma^{+}_{\omega_K} = \sum_{\pi\nu} \left[X^{\omega_K}_{\pi\nu} \alpha^{+}_{\nu} \alpha^{+}_{\bar{\pi}} + Y^{\omega_K}_{\pi\nu} \alpha_{\bar{\nu}} \alpha_{\pi} \right], \tag{1}$$

the intrinsic excited states $|\omega_K\rangle$ are given by

$$|\omega_K\rangle = \Gamma^{+}_{\omega_K}|0\rangle, \tag{2}$$

where the QRPA vacuum $|0\rangle$ satisfies

$$\Gamma_{\omega_K}|0\rangle = 0. \tag{3}$$

α^{+} and α are quasiparticle creation and annihilation operators, respectively. ω_K labels the QRPA excitation energy and $X^{\omega_K}_{\pi\nu}, Y^{\omega_K}_{\pi\nu}$ are the forward and backward amplitudes, respectively. In the intrinsic frame, the allowed GT transition amplitudes connecting the QRPA ground state to one-phonon states are given by

$$\langle \omega_K | \sigma_K t^{-} | 0 \rangle = \sum_{\pi\nu} \left(q_{\pi\nu} X^{\omega_K}_{\pi\nu} + \tilde{q}_{\pi\nu} Y^{\omega_K}_{\pi\nu} \right), \tag{4}$$

with

$$\tilde{q}_{\pi\nu} = u_\nu v_\pi \Sigma^{\nu\pi}_{K}, \quad q_{\pi\nu} = v_\nu u_\pi \Sigma^{\nu\pi}_{K}, \tag{5}$$

v's are occupation amplitudes ($u^2 = 1 - v^2$), and $\Sigma^{\nu\pi}_{K}$ spin matrix elements connecting neutron and proton states with spin operators,

$$\Sigma^{\nu\pi}_{K} = \langle \nu | \sigma_K | \pi \rangle. \tag{6}$$

Expressing the initial and final states in the laboratory frame in terms of the intrinsic states using the Bohr-Mottelson factorization [49], the GT strength $B_\omega(GT^-)$ for a transition $I_i K_i(0^+0) \rightarrow I_f K_f(1^+K)$ is obtained in terms of the intrinsic amplitudes in Eq. (4) as

$$B_\omega(GT^-) = \sum_{\omega_K} [\langle \omega_{K=0} | \sigma_0 t^{-} | 0 \rangle^2 \delta(\omega_{K=0} - \omega) + 2 \langle \omega_{K=1} | \sigma_1 t^{-} | 0 \rangle^2 \delta(\omega_{K=1} - \omega)], \tag{7}$$

in $[g_A^2/4\pi]$ units.

The GT strength distributions will be shown later as a function of the excitation energy E_{ex} with respect to the ground state of the odd-odd daughter nucleus, $E_{ex} = \omega_{\mathrm{QRPA}} - E_0$, obtained by subtracting the lowest two-quasiparticle energy E_0 from the calculated ω energy in the QRPA calculation.

β-decay half-lives are calculated by summing all the allowed transition strengths to states in the daughter nucleus with excitation energies lying below the corresponding Q energy, and weighted with the phase space factors $f(Z, Q_\beta - E_{ex})$,

$$T^{-1}_{1/2} = \frac{(g_A/g_V)^2_{\mathrm{eff}}}{D} \sum_{0<E_{ex}<Q_\beta} f(Z, Q_\beta - E_{ex}) B(GT, E_{ex}), \tag{8}$$

with $D = 6200$ s and $(g_A/g_V)_{\mathrm{eff}} = 0.77 (g_A/g_V)_{\mathrm{free}}$, where 0.77 is a standard quenching factor. The Q_{β^-} energy is given by

$$\begin{aligned} Q_{\beta^-} &= M(A,Z) - M(A,Z+1) - m_e \\ &= BE(A,Z) - BE(A,Z+1) + m_n - m_p - m_e, \end{aligned} \tag{9}$$

written in terms of the nuclear masses $M(A,Z)$ or nuclear binding energies $BE(A,Z)$ and the neutron (m_n), proton (m_p), and electron (m_e) masses.

The Fermi integral $f(Z, Q_\beta - E_{ex})$ is computed numerically for each value of the energy including screening and finite size effects, as explained in Ref. [50]. This function increases with the energy of the β particle and therefore the strength located at low excitation energies contributes more importantly to the half-life.

The β-delayed neutron-emission probability is calculated as

$$P_n = \frac{\sum_{S_n<E_{ex}<Q_\beta} f(Z, Q_\beta - E_{ex}) B(GT, E_{ex})}{\sum_{0<E_{ex}<Q_\beta} f(Z, Q_\beta - E_{ex}) B(GT, E_{ex})}. \tag{10}$$

Thus, P_n corresponds to the probability of neutron emission with no distinction between emission of one, two, or more neutrons. The sum extends to all the excited states in the daughter nucleus with excitation energies within the indicated ranges. S_n is the one-neutron separation energy in the daughter nucleus. In this expression it is assumed that all the decays to energies above S_n in the daughter nucleus lead to delayed neutron emission and then, γ decay from neutron unbound levels is neglected. Thus, the probability is always overestimated.

III. RESULTS AND DISCUSSION

Constrained HF+BCS calculations are performed to obtain energy curves that show the energy as a function of the quadrupole deformation β_2. Most of the energy curves in the isotopes studied in this work exhibit two local minima, prolate and oblate, separated by energy barriers that change with the neutron number. One can see in Fig. 1 the isotopic evolution of the quadrupole deformations for the prolate and oblate equilibrium shapes plotted versus the neutron number N. The results correspond to the unstable isotopes of the neutron-rich rare-earth nuclei considered in this work. The deformation of the ground state for each isotope is encircled. Prolate ground-state shapes are obtained in all the cases except some of the heavier isotopes that become oblate, and finally spherical when approaching the closed shell at $N = 126$. About the mid-shell one finds the largest deformations, as well as the largest energy barriers between the two minima. A very similar trend is observed in the profile of the curves in all the isotopic chains, showing larger deformations around mid-shell

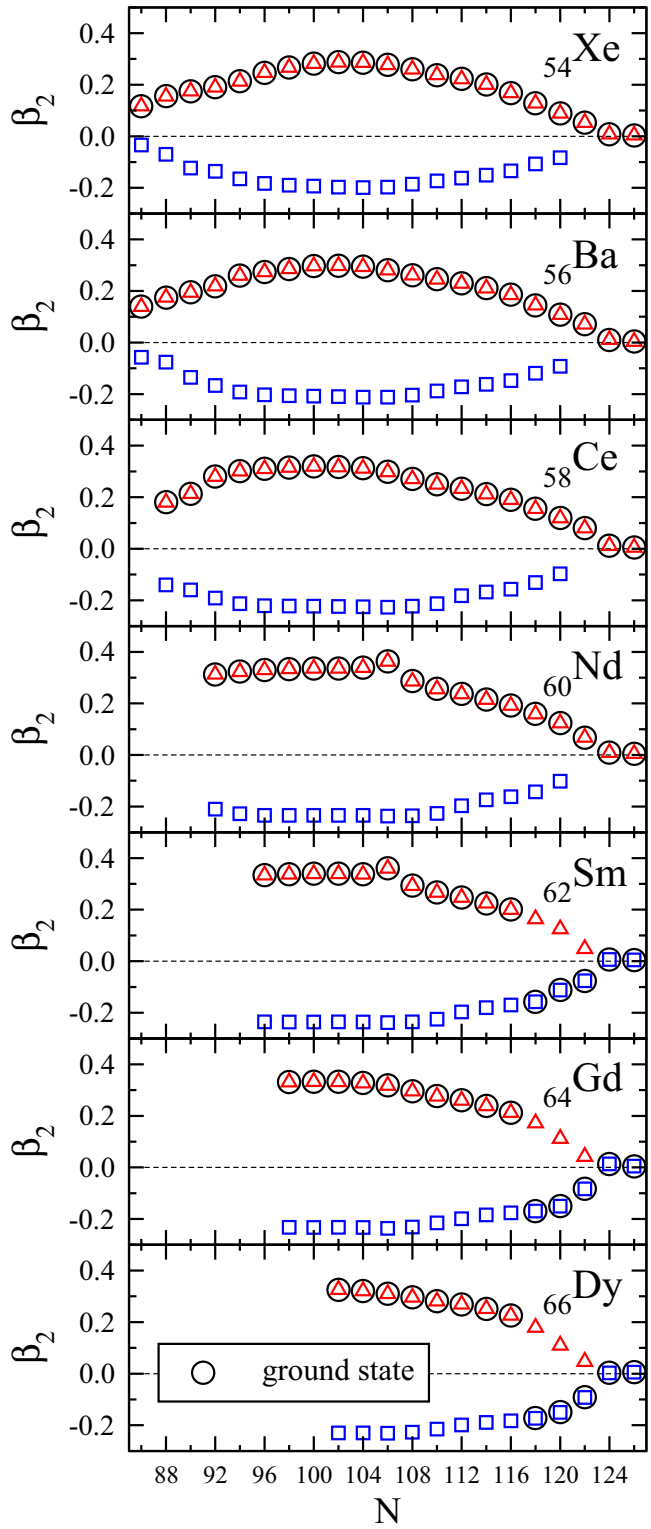

FIG. 1. Isotopic evolution of the quadrupole deformation β_2 corresponding to the energy minima in neutron-rich Xe, Ba, Ce, Nd, Sm, Gd, and Dy isotopes, obtained from SLy4. Ground-state results for each isotope are encircled.

($N = 104$) with values close to $\beta_2 = 0.35$ in the prolate sector and close to $\beta_2 = -0.25$ in the oblate one. The quadrupole deformations become smaller as one approaches the closed shell isotopes with $N = 82$ and $N = 126$. The deformations obtained in this work are in good agreement with those obtained with the Gogny-D1S energy density functional that are available in Ref. [51]. The shape transitions from prolate to oblate shapes is predicted to occur in this work between $N = 116$ and $N = 118$ in Sm, Gd, and Dy isotopes. This is in qualitative agreement with the results from Gogny-D1S, where the transitions are predicted at $N = 116$ in Sm and Gd and at $N = 114$ in Dy. Transitions at $N = 118$ in Nd and at $N = 120$ in Ce are also predicted with Gogny-D1S. It is also worth comparing the above results with those from modern global mass models, such as the semiempirical nuclear mass formula based on macroscopic-microscopic methods [52]. This mass formula predicts a shape transition from prolate to oblate at $N = 118$, 122, 122, 120, 118, 118, 116 in Xe, Ba, Ce, Nd, Sm, Gd, and Dy, respectively. Thus, the transition takes place somewhat earlier in the lighter nuclei Xe, Ba, Ce, and Nd, somewhat later in Sm and Gd, and at the same isotope $N = 116$ in Dy. Nevertheless, the important point is the shape-change tendency taking place before the closed shell at $N = 126$, which is a general feature of the isotopic shape evolution. The exact isotope where the transition takes place is not very relevant because the shape transition region is naturally characterized by very close energies in the prolate and oblate sector competing to each other to be ground states. Thus, small details of the calculations can change the energies and shift the ground state from one shape to another. Another odd effect observed in Fig. 1 is the presence of a little kink in the quadrupole deformations at $N = 106$ in Nd and Sm isotopes. This kink is related to a subtle effect that appears at mid-shell in these nuclei, where the tendency changes and the equilibrium deformation starts decreasing with increasing neutron number. Looking in detail into the energy-deformation curves obtained from constrained HF+BCS calculations, one finds out that this behavior is related to the topology of the curves in the prolate minimum. Whereas the minimum up to $N = 104$ is somewhat sharp, at $N = 106$ it becomes shallower with the absolute minimum at a somewhat larger value $\beta_2 = 0.36$. At $N = 108$ the prolate minimum is also somewhat shallow, but slightly peaked at a lower $\beta_2 = 0.29$. After that, it continuously decreases with increasing N. It is hard to find a simple explanation for this rare behavior that is related to a very subtle competition between the single-particle energies and their crossing as a function of deformation in these isotopes. The effect might also depend on the particular version of the Skyrme interaction used (SLy4 in this case).

In the next figure (Fig. 2) the accumulated GT strength, that is, the GT strength contained up to a given excitation energy, is plotted as a function of the excitation energy of the daughter nucleus. A quenching factor 0.77 was included in the results. The figures cover the energy range below the Q_β energy, which is the relevant region for the calculation of the half-lives. Only the results for the lighter unstable isotopes are shown because they offer better possibilities to be measured. Vertical arrows indicate the experimental Q_β energies [41].

The energy distribution of the GT strength is fundamental to constrain the underlying nuclear structure involved in the calculation of the the half-lives. The decay rates in astrophysical scenarios may, however, be different from the

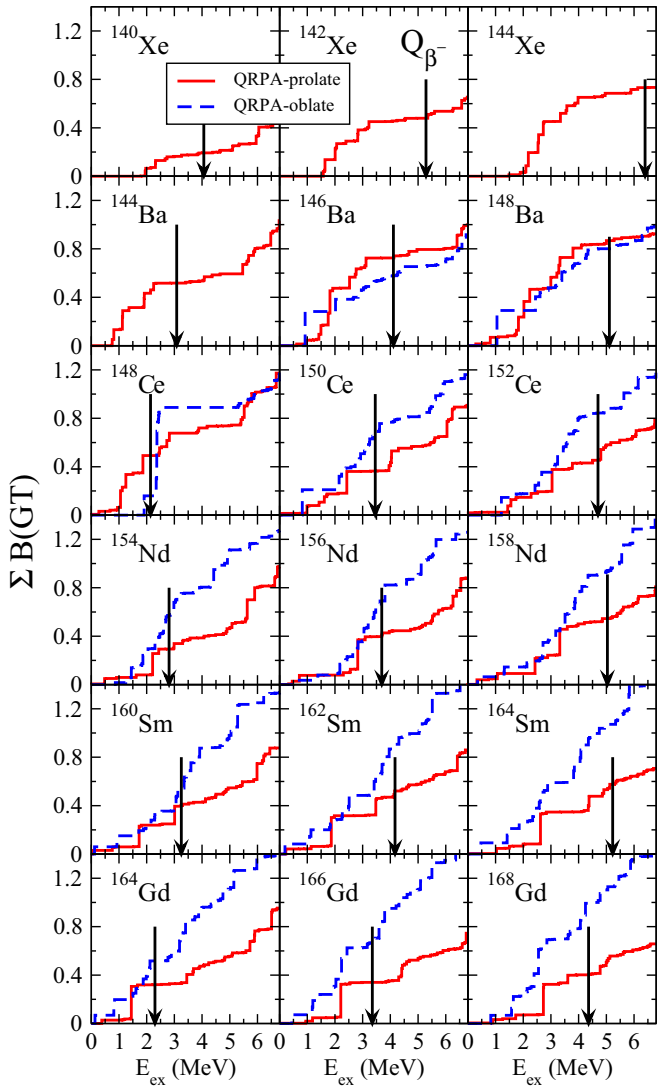

FIG. 2. QRPA-SLy4 accumulated GT strengths in various Xe, Ba, Ce, Nd, Sm, Gd, and Dy isotopes calculated for the prolate and oblate equilibrium shapes. Q_β energies are shown with vertical arrows.

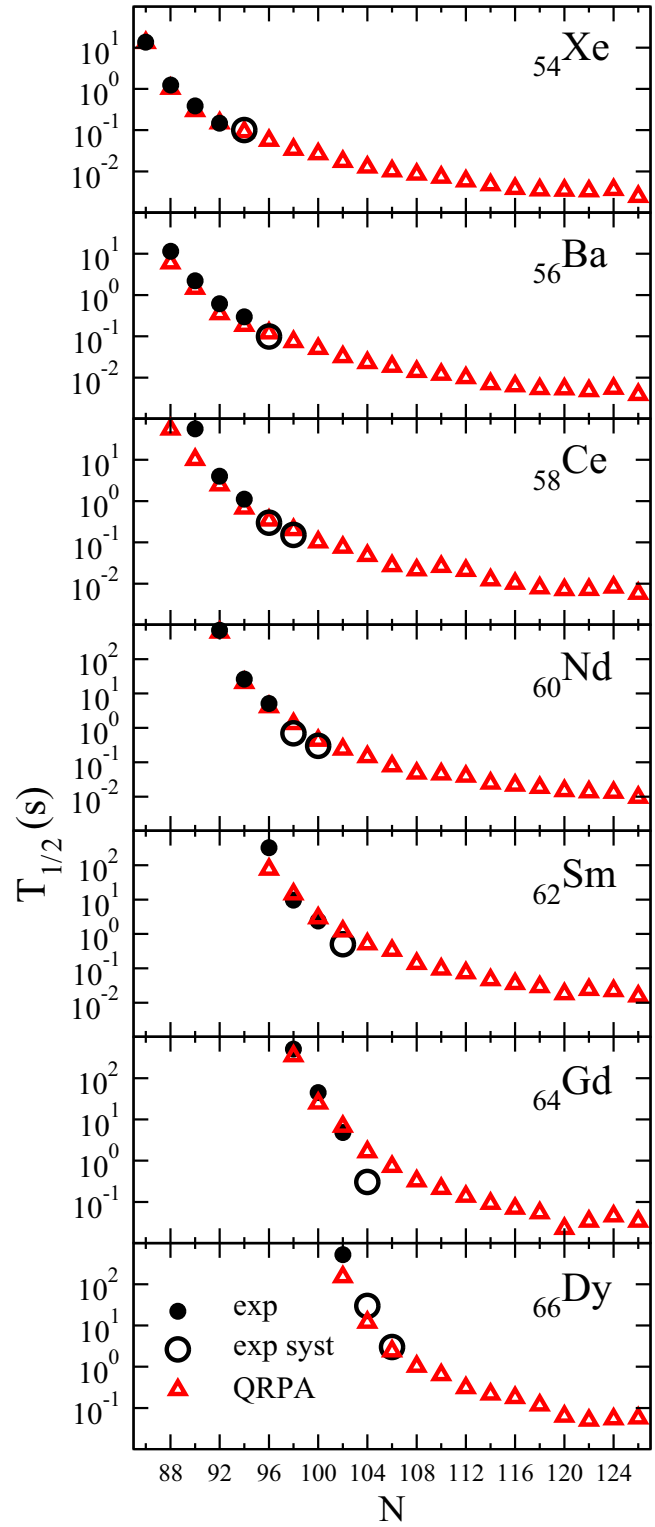

FIG. 3. Theoretical QRPA-SLy4 β-decay half-lives compared with experimental half-lives [41] (open circles stand for experimental values from systematics) for neutron-rich Xe, Ba, Ce, Nd, Sm, Gd, and Dy isotopes.

decay rates in the laboratory because the phase factors may be also different. Therefore, to describe properly the decay rates under extreme conditions of density and temperature, it is not sufficient to reproduce the half-lives in the laboratory. One needs, in addition, to have a reliable description of the GT strength distributions [45,46]. The different profiles observed for the prolate and oblate nuclear shapes is a typical example of the sensitivity of the GT strength distribution to deformation. This sensitivity is translated into the β-decay half-lives. In the heavier isotopes Ce, Nd, Sm, and Gd, the oblate shapes generate more GT strength than the prolate ones at low excitation energies and as a result, the oblate shapes produce shorter half-lives. Experimental information on these strength distributions will be very valuable to constrain further the nuclear structure calculations.

The calculation of the half-lives in Eq. (8) relies on the GT strength distribution and Q_β values. In this work, values obtained from SLy4 [53] are used. In Fig. 3 the measured β-decay half-lives (solid dots), including the values extracted from systematics (open dots) [41], are compared with the theoretical results of this work for the various isotopic

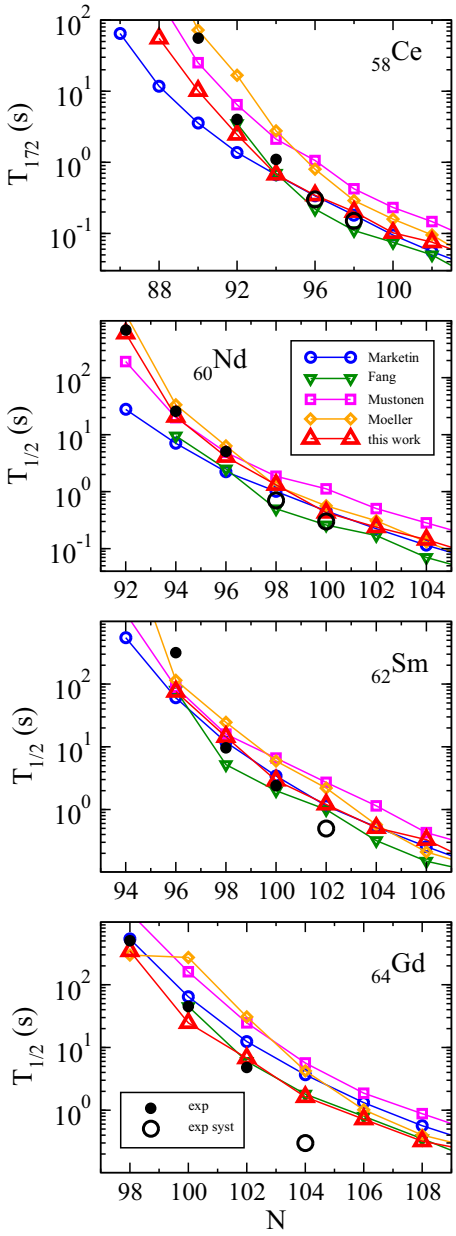

FIG. 4. Theoretical QRPA-SLy4 β-decay half-lives (this work) compared with results from Marketin *et al.* [40], Fang [38], Mustonen *et al.* [39], and Moeller *et al.* [37]. Experimental data are as in Fig. 3.

chains. In general, a very reasonable agreement with the few experimental measurements in this mass region is obtained.

In Fig. 4 I compare the results for the half-lives obtained in this work with the results in Refs. [37–40] and with experiment. Results are shown for the Ce, Nd, Sm, and Gd isotopes around the region where the half-lives are measured. The calculations in Ref. [37] combine a microscopic QRPA approach based on a Yukawa single-particle Hamiltonian and a separable residual interaction in the ph channel for the GT response with the statistical gross theory for the first-forbidden decay [37]. The Q_β and neutron separation energies are taken from the masses calculated in the finite-range droplet model (FRDM) [54]. The calculations are done without any quenching of the axial-vector coupling constant g_A. The results in Ref. [38] are obtained from deformed QRPA calculations based on Woods-Saxon potentials and realistic CD-Bonn residual forces using the G matrix. The strength of the pp residual interaction is renormalized by taking into account the Pauli exclusion principle that generalizes the usual quasiboson approximation. This procedure avoids using effective parametrizations of the the pp force. The masses are also taken from the FRDM [54] and a standard quenching is included. Global calculations of decay properties based on Skyrme QRPA for axially deformed even-even nuclei have been performed in Ref. [39] within the finite-amplitude method. Allowed and FF transitions are both considered. The results in Ref. [40] correspond to spherical calculations within a relativistic formalism including FF transitions. In the last two cases the masses are calculated consistently, but whereas the quenching of g_A is considered for both GT and FF transitions in Ref. [40], it is only included for GT transitions in Ref. [39].

Figure 4 shows that the half-lives calculated in Refs. [37] and [39] have a tendency to be above the half-lives calculated in Refs. [40] and [38]. The calculations in this work appear between the results of the other approaches, except in the case of Gd isotopes, where they are lower. The agreement with experiment is comparable in the various calculations. The various calculations differ as much as one order of magnitude depending on the nucleus. Then, this is the expected spreading of the half-lives caused by different approaches and by uncertainties associated with the various approximations and choice of parameters. Certainly, it will be very interesting to extend the measurements of half-lives in this mass region.

The effect of the FF contributions is still controversial and seems to be very different in different mass regions. Whereas they represent minor effects in regions around $N = 50$, their effect could be more important around $N = 82$ and especially in $N = 126$ [29,55,56]. Several calculations include first-forbidden transitions in the rare-earth mass region [37,39,40], but the results are in many cases completely at variance.

Figure 5 shows the results for the β-delayed neutron-emission probabilities, expressed as percentages. These are the ratios of the rates from transitions above the neutron separation energy S_n to the total β-decay rates. As it is defined, P_n includes the β-delayed probabilities for the emission of any number of neutrons. P_n is a sensitive function of both S_n and Q_β energies, which are evaluated from the SLy4 Skyrme force [53].

The lighter isotopes in all the isotopic chains in Fig. 5 are close to stability and have S_n energies larger than Q_β energies. Therefore, the P_n values are obviously zero. As one moves away from stability, heavier isotopes exhibit decreasing S_n energies and increasing Q_β energies and as a result, P_n values start to increase accordingly. The neutron number N at which P_n starts to increase corresponds to the isotopes where $S_n \simeq Q_\beta$. This neutron number increases with the number of protons and changes slightly depending on the model. In Fig. 5 the results in this work are compared with both the results from relativistic calculations of Ref. [40] and from the microscopic-macroscopic calculations of Ref. [37]. The increasing of P_n with the nuclear instability is a general pattern in all the calculations, but whereas the results in this

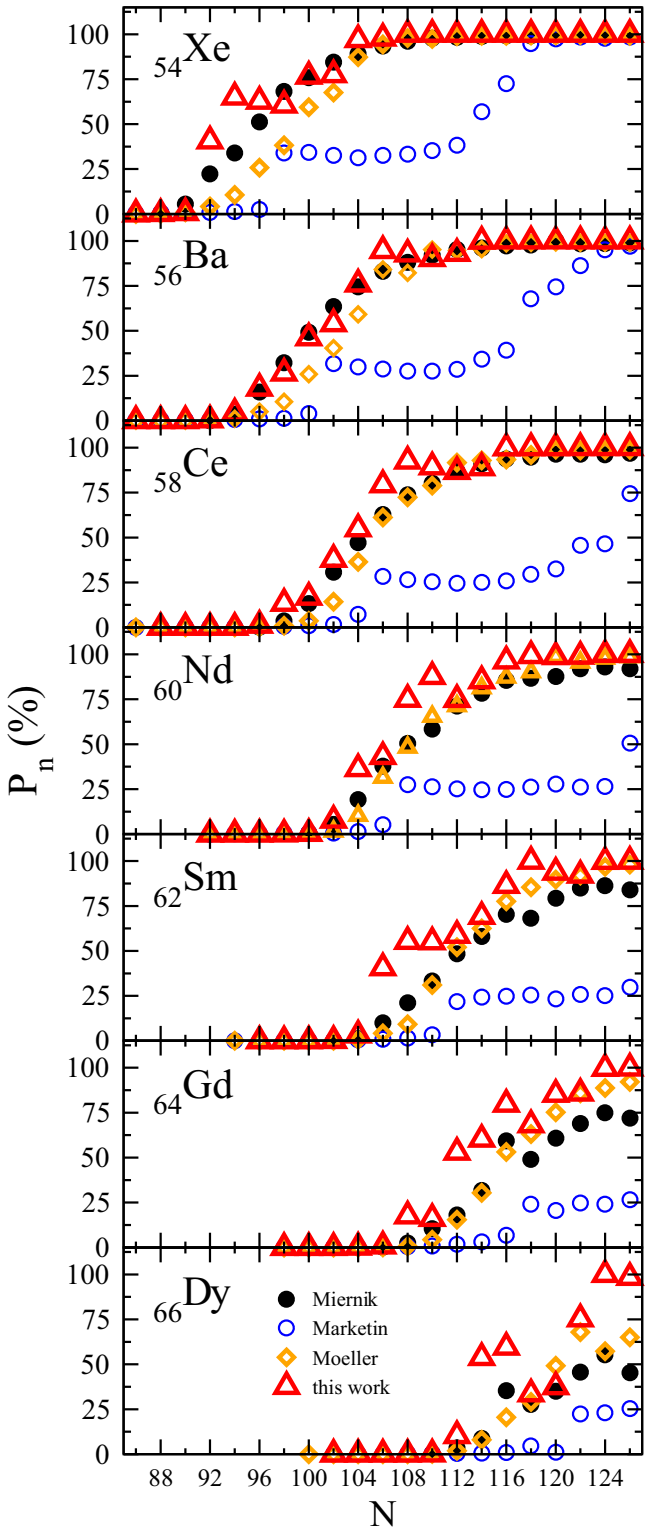

FIG. 5. Theoretical QRPA-SLy4 percentage values of the probability for β-delayed neutron emission P_n. Results in this work are compared with those of Marketin *et al.* [40] and Moeller *et al.* [37], as well as with the phenomenological model by Miernik [57].

work follow the same tendency as the results in Ref. [37], the P_n values from the relativistic calculations are systematically lower. The direct consequence would be that less free neutrons are predicted in the astrophysical scenarios where these nuclei are decaying. Unfortunately, the experimental information on P_n values in this mass region of interest for the r process is still very limited because of the low production rates of exotic nuclei and the difficulties inherent in neutron detection. Indeed, there are no P_n measurements available in the nuclei studied in this work. Thus, it is worth comparing the results obtained here with those of a phenomenological model based on a statistical level density function. This model [57] was shown to reproduce the available experimental β-delayed neutron-emission probabilities to an equivalent or better degree than previous models. The results shown in Fig. 5 with black dots correspond to this model [57] based on theoretical masses from HFB-21 [58] for the calculation of Q_β and neutron separation energies. The isotopic pattern is in general fairly well reproduced, although the detailed behavior in the region of increasing P_n contains more fluctuations in the present calculations.

IV. CONCLUSIONS

I have calculated β-decay properties of even-even neutron-rich isotopes in the rare-earth mass region. These nuclei are expected to play an important role in the nucleosynthesis r process and in particular, they are crucial to understand the existence of the rare-earth peak in the pattern of isotopic abundances. Namely, isotopes of Xe, Ba, Ce, Nd, Sm, Gd, and Dy with neutron numbers between $N = 86$ and $N = 126$ are included in this study.

A theoretical approach based on deformed HF+BCS+QRPA calculations with Skyrme effective interactions and separable residual forces is used to obtain GT strength distributions, β-decay half-lives, and β-delayed neutron-emission probabilities. The results from this approach are compared with the available experimental information and with calculations based on different methods. In general, a reasonable agreement with experiment is obtained. The results are comparable to other calculations using different approaches, different mean fields or different residual interactions.

These calculations are timely because they address a mass region which is at the borderline of present experimental capabilities. Experimental information on the energy distribution of the GT strength is a valuable piece of knowledge about the nuclear structure in this mass region. The study of these distributions is within the current experimental capabilities in the case of the lighter isotopes considered in this work. Here, theoretical predictions have been presented for them based on microscopic calculations. Similarly, measuring the half-lives of the heavier isotopes will be highly beneficial to model the r process and to constrain theoretical nuclear models. These measurements are also a real possibility within present capabilities at MSU and RIKEN.

A data set containing the main results of this work is available as Supplemental Material [59] to this article.

ACKNOWLEDGMENTS

I thank K. Yoshida for useful discussions. This work was supported by Ministerio de Economía y Competitividad (Spain) under Contract No. FIS2014-51971-P.

[1] E. M. Burbidge, G. M. Burbidge, W. A. Fowler, and F. Hoyle, Rev. Mod. Phys. **29**, 547 (1959).
[2] J. J. Cowan, F.-K. Thielemann, and J. W. Truran, Phys. Rep. **208**, 267 (1991).
[3] M. Arnould, S. Goriely, and K. Takahashi, Phys. Rep. **450**, 97 (2007).
[4] Y.-Z. Qian and G. J. Wasserburg, Phys. Rep. **442**, 237 (2007).
[5] M. R. Mumpower, G. C. McLaughlin, and R. Surman, Phys. Rev. C **85**, 045801 (2012).
[6] M. R. Mumpower, R. Surman, D.-L. Fang, M. Beard, P. Möller, T. Kawano, and A. Aprahamian, Phys. Rev. C **92**, 035807 (2015).
[7] R. Surman, J. Engel, J. R. Bennett, and B. S. Meyer, Phys. Rev. Lett. **79**, 1809 (1997).
[8] M. Mumpower, J. Cass, G. Passucci, R. Surman, and A. Aprahamian, AIP Advaces **4**, 041009 (2014).
[9] S. Goriely, J.-L. Sida, J.-F. Lemaître, S. Panebianco, N. Dubray, S. Hilaire, A. Bauswein, and H.-T. Janka, Phys. Rev. Lett. **111**, 242502 (2013).
[10] http://research.jyu.fi/igisol/JYFLTRAP_masses/.
[11] J. Pereira, S. Hennrich, A. Aprahamian, O. Arndt, A. Becerril, T. Elliot, A. Estrade, D. Galaviz, R. Kessler, K.-L. Kratz, G. Lorusso, P. F. Mantica, M. Matos, P. Möller, F. Montes, B. Pfeiffer, H. Schatz, F. Schertz, L. Schnorrenberger, E. Smith, A. Stolz, M. Quinn, W. B. Walters, and A. Wöhr, Phys. Rev. C **79**, 035806 (2009).
[12] S. Nishimura, Z. Li, H. Watanabe, K. Yoshinaga, T. Sumikama, T. Tachibana, K. Yamaguchi, M. Kurata-Nishimura, G. Lorusso, Y. Miyashita, A. Odahara, H. Baba, J. S. Berryman, N. Blasi, A. Bracco, F. Camera, J. Chiba, P. Doornenbal, S. Go, T. Hashimoto, S. Hayakawa, C. Hinke, E. Ideguchi, T. Isobe, Y. Ito, D. G. Jenkins, Y. Kawada, N. Kobayashi, Y. Kondo, R. Krücken, S. Kubono, T. Nakano, H. J. Ong, S. Ota, Z. Podolyák, H. Sakurai, H. Scheit, K. Steiger, D. Steppenbeck, K. Sugimoto, S. Takano, A. Takashima, K. Tajiri, T. Teranishi, Y. Wakabayashi, P. M. Walker, O. Wieland, and H. Yamaguchi, Phys. Rev. Lett. **106**, 052502 (2011).
[13] G. Lorusso *et al.*, Phys. Rev. Lett. **114**, 192501 (2015).
[14] M. Quinn, A. Aprahamian, J. Pereira, R. Surman, O. Arndt, T. Baumann, A. Becerril, T. Elliot, A. Estrade, D. Galaviz, T. Ginter, M. Hausmann, S. Hennrich, R. Kessler, K. L. Kratz, G. Lorusso, P. F. Mantica, M. Matos, F. Montes, B. Pfeiffer, M. Portillo, H. Schatz, F. Schertz, L. Schnorrenberger, E. Smith, A. Stolz, W. B. Walters, and A. Wöhr, Phys. Rev. C **85**, 035807 (2012).
[15] R. Reifarth *et al.*, J. Phys.: Conf. Ser. **665**, 012044 (2016).
[16] J. Wu *et al.*, EPJ Web Conf. **109**, 08003 (2016).
[17] C. Wrede, EPJ Web Conf. **93**, 07001 (2015).
[18] J. Engel, M. Bender, J. Dobaczewski, W. Nazarewicz, and R. Surman, Phys. Rev. C **60**, 014302 (1999).
[19] I. N. Borzov, J. J. Cuenca-García, K. Langanke, G. Martínez-Pinedo, and F. Montes, Nucl. Phys. A **814**, 159 (2008).
[20] T. Niksic, T. Marketin, D. Vretenar, N. Paar, and P. Ring, Phys. Rev. C **71**, 014308 (2005).
[21] J. Krumlinde and P. Möller, Nucl. Phys. A **417**, 419 (1984).
[22] H. Homma, E. Bender, M. Hirsch, K. Muto, H. V. Klapdor-Kleingrothaus, and T. Oda, Phys. Rev. C **54**, 2972 (1996).
[23] K. Muto, E. Bender, T. Oda, and H. V. Klapdor-Kleingrothaus, Z. Phys. A **341**, 407 (1992).
[24] F. Frisk, I. Hamamoto, and X. Z. Zhang, Phys. Rev. C **52**, 2468 (1995).
[25] P. Sarriguren, E. Moya de Guerra, A. Escuderos, and A. C. Carrizo, Nucl. Phys. A **635**, 55 (1998).
[26] P. Sarriguren, E. Moya de Guerra, and A. Escuderos, Nucl. Phys. A **691**, 631 (2001).
[27] P. Sarriguren, E. Moya de Guerra, and A. Escuderos, Nucl. Phys. A **658**, 13 (1999).
[28] P. Sarriguren, E. Moya de Guerra, and A. Escuderos, Phys. Rev. C **64**, 064306 (2001).
[29] D. L. Fang, B. A. Brown, and T. Suzuki, Phys. Rev. C **88**, 024314 (2013).
[30] D. Ni and Z. Ren, Phys. Rev. C **89**, 064320 (2014); J. Phys. G: Nucl. Part. Phys. **39**, 125105 (2012).
[31] K. Yoshida, Prog. Theor. Exp. Phys. (2013) 113D02.
[32] M. Martini, S. Péru, and S. Goriely, Phys. Rev. C **89**, 044306 (2014).
[33] E. Nácher, A. Algora, B. Rubio, J. L. Taín, D. Cano-Ott, S. Courtin, P. Dessagne, F. Maréchal, C. Miehé, E. Poirier, M. J. G. Borge, D. Escrig, A. Jungclaus, P. Sarriguren, O. Tengblad, W. Gelletly, L. M. Fraile, and G. Le Scornet, Phys. Rev. Lett. **92**, 232501 (2004); E. Poirier, F. Maréchal, P. Dessagne, A. Algora, M. J. G. Borge, D. Cano-Ott, J. C. Caspar, S. Courtin, J. Devin, L. M. Fraile, W. Gelletly, G. Heitz, A. Jungclaus, G. Le Scornet, C. Miehé, E. Nácher, B. Rubio, P. Sarriguren, J. L. Taín, O. Tengblad, and C. Weber (the ISOLDE Collaboration), Phys. Rev. C **69**, 034307 (2004); A. Pérez-Cerdán *et al.*, *ibid.* **88**, 014324 (2013); M. E. Estévez Aguado *et al.*, *ibid.* **92**, 044321 (2015).
[34] P. Sarriguren and J. Pereira, Phys. Rev. C **81**, 064314 (2010).
[35] P. Sarriguren, A. Algora, and J. Pereira, Phys. Rev. C **89**, 034311 (2014).
[36] P. Sarriguren, Phys. Rev. C **91**, 044304 (2015).
[37] P. Möller, B. Pfeiffer, and K.-L. Kratz, Phys. Rev. C **67**, 055802 (2003).
[38] D.-L. Fang, Phys. Rev. C **93**, 034306 (2016).
[39] M. T. Mustonen and J. Engel, Phys. Rev. C **93**, 014304 (2016).
[40] T. Marketin, L. Huther, and G. Martínez-Pinedo, Phys. Rev. C **93**, 025805 (2016).
[41] G. Audi *et al.*, Chinese Physics C **36**, 1157 (2012); **36**, 1603 (2012).
[42] K. Langanke and G. Martínez-Pinedo, Nucl. Phys. A **673**, 481 (2000).
[43] E. Chabanat, P. Bonche, P. Haensel, J. Meyer, and R. Schaeffer, Nucl. Phys. A **635**, 231 (1998).
[44] J. M. Boillos and P. Sarriguren, Phys. Rev. C **91**, 034311 (2015).
[45] P. Sarriguren, Phys. Rev. C **79**, 044315 (2009).
[46] P. Sarriguren, Phys. Lett. B **680**, 438 (2009).
[47] M. S. Yousef, V. Rodin, A. Faessler, and F. Šimkovic, Phys. Rev. C **79**, 014314 (2009).
[48] D. Fang, A. Faessler, V. Rodin, M. S. Yousef, and F. Šimkovic, Phys. Rev. C **81**, 037303 (2010).
[49] A. Bohr and B. Mottelson, *Nuclear Structure*, Vols. I and II, (Benjamin, New York 1975).
[50] N. B. Gove and M. J. Martin, Nucl. Data Tables **10**, 205 (1971).
[51] S. Hilaire and M. Girod, Eur. Phys. J. A **33**, 237 (2007); www-phynu.cea.fr/science_en_ligne/carte_potentiels_microscopiques/carte_potentiel_nucleaire_eng.htm.
[52] Ning Wang, Min Liu, and Xizhen Wu, Phys. Rev. C **81**, 044322 (2010); Min Liu, Ning Wang, Yangge Deng, and Xizhen Wu, *ibid.* **84**, 014333 (2011).
[53] M. V. Stoitsov, J. Dobaczewski, W. Nazarewicz, and P. Ring, Comp. Phys. Comm. **167**, 43 (2005).

[54] P. Möller, J. R. Nix, W. D. Myers, and W. J. Swiatecki, At. Data Nucl. Data Tables **59**, 185 (1995).
[55] I. N. Borzov, Phys. Rev. C **67**, 025802 (2003).
[56] Q. Zhi, E. Caurier, J. J. Cuenca-García, K. Langanke, G. Martínez-Pinedo, and K. Sieja, Phys. Rev. C **87**, 025803 (2013).
[57] K. Miernik, Phys. Rev. C **88**, 041301(R) (2013); **90**, 054306 (2014); https://github.com/kmiernik/delayed_neutrons.
[58] S. Goriely, N. Chamel, and J. M. Pearson, Phys. Rev. C **82**, 035804 (2010).
[59] See Supplemental Material at http://link.aps.org/supplemental/10.1103/PhysRevC.95.014304 for a data set containing quadrupole deformations, GT strength distributions, β-decay half-lives, and β-delayed neutron emission probabilities for all isotopes considered in this study.